Am J Cancer Res 2024;14(7):3451-3467
www.ajcr.us /ISSN:2156-6976/ajcr0155647

Original Article

PDE4B promotes the progression of gastric cancer via the PI3K/AKT/MYC pathway and immune infiltration

Riya Su[1], Narenmandula[2], Xiaojuan Qiao[3], Qun Hu[3]

[1]Department of Pharmacology, Zhongshan School of Medicine, Sun Yat-sen University, No. 74 Zhongshan Second Road, Yuexiu District, Guangzhou 510080, Guangdong, China; [2]School of Traditional Mongolian Medicine, Inner Mongolia Medical University, Jinshan Development Zone, Hohhot 010110, Inner Mongolia, China; [3]Department of Oncology, Affiliated Hospital of Inner Mongolia Medical University, No. 1 Tongdao North Road, Hohhot 010050, Inner Mongolia, China

Received January 27, 2024; Accepted June 25, 2024; Epub July 15, 2024; Published July 30, 2024

Abstract: Phosphodiesterase 4B (PDE4B) is a key enzyme involved in regulating intracellular cyclic adenosine monophosphate levels and plays a significant role in the diagnosis, classification, treatment, and prognosis of various cancers. However, the role of PDE4B in gastric cancer (GC) remains unclear. We used the GEPIA2 (Gene Expression Profiling Interactive Analysis 2) database to analyze the differential expression level of PDE4B across tumor samples and verified our findings via qPCR and immunohistochemical analysis. We also analyzed the correlation between PDE4B expression levels and clinical pathological parameters, and prognosis, in the database. The effects of PDE4B on GC proliferation, migration, and invasion were evaluated through in vitro and in vivo experiments. Enrichment analysis was performed using bioinformatic tools, and results were validated by western blot analysis. The correlation between PDE4B expression and immune cell infiltration was investigated using bioinformatics tools. PDE4B is highly expressed in GC and is significantly associated with deep infiltration, distant metastasis, tumor, node, metastasis (TNM) stage, and preoperative CA199 levels. Over-expression of PDE4B promotes proliferation, clonal formation, migration, and invasion of GC cells and is associated with poor prognosis. PDE4B promotes the infiltration of immune cells into the tumor microenvironment (TME) and the phosphorylation of PI3K/AKT pathway, increasing MYC expression. PDE4B can serve as an independent prognostic biomarker for GC. We found that PDE4B can promote immune cell infiltration of the TME and mediate malignancy in gastric cancer through the PI3K/AKT/MYC pathway.

Keywords: Gastric cancer, immune infiltration, metastasis, PDE4B, PI3K/AKT, MYC, proliferation

Introduction

Gastric cancer (GC) is a globally significant disease, with the majority of new cases diagnosed in developing countries [1]. In China, GC ranks as the second most prevalent cancer. Early-stage GC often lacks discernible symptoms, and by the time symptoms manifest, the disease is frequently advanced and incurable, resulting in a high mortality rate [2, 3]. The current treatment options for GC primarily include surgery, radiotherapy, and chemotherapy; however, the incidence of local recurrence or distant metastasis after surgery exceeds 40% [4], leading to a 5-year survival rate of only 20%-40% for GC patients [5]. Consequently, the development of new, less invasive biomarkers for the early detection and prognostic prediction of GC is imperative to curing this disease and improving patients' quality of life.

Phosphodiesterase 4 (PDE4) controls the hydrolysis and degradation of cyclic adenosine monophosphate (cAMP). Four PDE4 genes (PDE4A-PDE4D) have been identified, each encoding different subtypes of the enzyme [6]. PDE4 is widely expressed in inflammatory cells. PDE4 Inhibitors have demonstrated anti-inflammatory activity and are used in the treatment of conditions such as psoriasis [7], systemic sclerosis [8], asthma, chronic obstructive pulmonary disease [9] and idiopathic pulmonary fibrosis [10]. PDE4B specifically inactivates the secondary messenger cAMP, preventing apoptosis

and promoting cell survival and proliferation [11]. PDE4B has been found to limit apoptosis in diffuse large B-cell lymphoma [12] and is associated with reduced apoptosis and increased metastasis in both renal carcinoma [13] and endometrial carcinoma [14]. Studies have confirmed that PDE4B is a promising candidate as a therapeutic target and prognostic molecular marker in colorectal cancer (CRC) [15]. However, the expression and regulation of PDE4B in GC, and its correlation with clinical treatment and prognosis, remain unclear.

The objective of this study was to determine the role of PDE4B in GC. We examined the differences in PDE4B expression between GC tumor cells and normal cells. Furthermore, we analyzed the correlation between PDE4B levels and clinicopathological characteristics of GC patients. We manipulated PDE4B expression in vitro and evaluated its impact on the biological behavior of GC cells. Finally, we demonstrated that variation in PDE4B expression affects GC progression via the PI3K/AKT/MYC pathway. Our findings suggest that PDE4B may be a suitable prognostic biomarker and a new therapeutic target for GC patients in the future.

Materials and methods

PDE4B expression in database

We used the "Expression analysis-Box Plots" module of GEPIA2 database[16] (http://gepia2.cancer-pku.cn) to get the box diagrams of differential expressions of tumor tissues and normal tissues in GTEx (genotype-tissue expression) database, including 408 STAD (stomach adenocarcinoma) tissues and 211 normal gastric tissues. We obtained the violin charts of PDE4B expression in all TCGA cancer tissues in different pathological stages (stage I, stage II, stage III and stage IV) through GEPIA2's "Pathological Stage Plot" module.

Analysis of survival prognosis in database

We utilized the survival analysis module of GEPIA2 to obtain the significant maps of overall survival (OS) data. The high cut-off value (50%) and the low cut-off value (50%) were used as the expression thresholds to divide the samples into high-expression and low-expression groups, and the critical value was set as median. The hypothesis testing was performed using the log-rank test.

Human gastric tissue samples

The pathological specimens used in this study were collected from the Pathology Department of Bayannur Hospital between February 2006 and January 2016. A total of 666 tissue samples were obtained from patients after surgery or gastric endoscopic biopsy, including 501 GC tissues and 165 paired para-carcinoma tissues. None of the volunteers undergone any chemotherapy or radiotherapy before surgery or biopsy. Histopathological confirmation of tissues was performed by two pathologists blinded to each other. Clinicopathological data such as age, tumor size, grade and TNM stage were collected from patients' medical records. This study adhered to medical ethical standards and was approved by the Ethics Committee of Inner Mongolia Medical University. Written informed consent was obtained from all participants in the study.

Tissue microarray (TMA) construction and immunohistochemistry (IHC)

All tissue samples were fixed with 4% formalin and embedded in paraffin. The TMA was constructed with paraffin-embedded blocks of donor tissues. Cores biopsies of 3 mm in diameter acquired from donor blocks were cut into 3 μm thicknesses. Sections of the tissue blocks were placed on glass slides and deparaffinized in gradient ethanol. The TMA was subjected to antigen retrieval by heating in citrate buffer (0.01 M, pH6.0), followed by blocking of endogenous peroxidase activity using 3% H_2O_2. The sections were then incubated with rabbit anti PDE4B polyclonal primary antibodies and stained. Sections were stained after incubated with an anti-PDE4B polyclonal primary antibody. The staining intensity was scored on a scale of 0 (negative), 1 (weakly positive), 2 (moderately positive), and 3 (strongly positive). The final score was calculated as 100× the product of the staining intensity and the percentage of stained cells.

Evaluation of the PDE4B immunohistochemical (IHC) staining was performed by two pathologists who were blinded to patient information. The cutoff value was determined as 195 by the X-tile-based TMA data analysis. Scores between 0 and 195 represented low expression of PDE4B, while scores between 196 and 300 represented high expression of PDE4B.

Stable cell lines

The human GC cell lines MNK-1, HGC-27 and human gastric mucosal cell line GES-1 were cultured in an incubator at 37°C with 5% CO_2. Purchase lentivirus-based shRNA targeting PDE4B and lentivirus vector. The GC cell lines HGC-27 were respectively infected with the lentivirus expressing shNC or shPDE4B. Lentivirus-mediated PDE4B-cDNA were transfected into MNK-1 cells, resulting in the creation of two cell lines: ovPDE4B and ovNC.

qRT-PCR

To detect PDE4B mRNA expression, total RNA was extracted from cells, and then the cDNA was synthesized through reverse transcription. The human PDE4B primers used were as follows: forward 5'-CAAGCATCTCACGCTTTGGAG-3', and reverse 5'-GCCACGTCAGAATGGTAATGG-3'. The human GAPDH primers were as follows: forward 5'-CTGGGCTACACTGAGCACC-3', and reverse 5'-AAGTGGTCGTTGAGGGCAATG-3'. The Ct values for the PDE4B genes were compared to the Ct values for GAPDH, which served as an internal control gene. Each experiment was conducted three times in total. The relative expression was calculated using the 2^(-ΔΔCt) technique.

Western blot

Extract total proteins from different stable cells using RIPA buffer. Protein samples were degenerated at 100°C for 10 min after being mixed with loading buffer. The same amounts of proteins were separated by sodium dodecyl sulfate-polyacrylamide gel electrophoresis (SDS-PAGE) and transferred to a polyvinylidene fluoride (PVDF) membrane. Incubate the membrane with primary antibodies of PDE4B, P-PI3K, PI3K, P-AKT, AKT, MYC, GAPDH, CD19, CD117 and SMA at 4°C overnight. After three rinses with PBST buffer for 15 min each time, incubate the membrane with horseradish-peroxidase-labeled secondary antibody at room temperature for 2 h. Then, the membrane was rinsed with PBST and developed.

CCK-8 assay

A total of 2000 cancer cells were added into each well of 96-well plate. Next, 10 μL of CCK-8 solution was added to each well, and the absorbance of each well was measured at 450 nm after incubated at 37°C for 2 h. The cells were plated in 96-well plate at a density of 5×10^3 cells/well for each experimental group. The cell proliferation level was assessed at 24 h, 48 h, 72 h, and 96 h, respectively. The cells in each well were incubated with a 100 μl mixture of medium and CCK-8 reagent (9:1), followed by measuring the absorbance at OD450 using a microplate reader after incubating at 37°C in the dark for 2 h.

Clone formation assay

The cells of each group were planted in a 6-well plate with 1000 cells/well. The plate was cultured in an incubator with 5% CO_2 at 37°C for 2 w. The culture medium was changed every 72 h. Then the cells were rinsed with PBS buffer three times gently and soaked in 4% paraformaldehyde for 30 min. The cells were incubated with 0.5% crystal violet solution at room temperature for 30 min. Finally, the cell clones were rinsed by ddH_2O.

Trans-well assays

Migration assay: Suspend cells in serum-free medium and plant in the upper chamber of Trans-well insert. Place the Trans-well chamber in a 24-well plate containing filled with medium containing 20% FBS. Incubate the cells in the incubator for 24 h. Gently remove the cells in the upper chamber using a cotton swab. Fix the chamber with 4% paraformaldehyde for 30 min, then stain the cells with 0.2% crystal violet for 30 min. After rinsing and drying, observe cell clones and count them.

Invasion analysis: Dilute the Matrigel basement membrane matrix in a 1:3 ratio using serum-free culture medium at 4°C. Add 100 μl of the matrix mixture onto the surface of the upper chamber and dry at 37°C for 1 h. The subsequent steps are the same as those of the migration assay described previously.

Flow cytometry method

Firstly, collect all cells and wash off EDTA. After resuspend with PBS, centrifuge at 1000 rpm for 5 min and discard the supernatant. And resuspend with 200 μl Binding Buffer, then incubate at room temperature in dark for 10 min after add 5 μl Annexin V-FITC. Then, at

1000 rpm, centrifuge for 5 minutes and discard the supernatant. After resuspend with 200 μl Binding Buffer and add 5 μl PI staining, it was detected.

Subcutaneous tumor model

A total of 12 five-week-old male BALB/C nude immunodeficient mice were used in the study. Cells of the MNK-1 group were suspended at a density of 1×10^7 cells/ml. Cell suspensions (150 μl) were injected into the armpit region of the left upper extremity of the mice, and tumor weight was measured.

The tumor volume was calculated as longest diameter × shortest diameter^2/2.

Gene set and functional enrichment analysis

The WGCNA algorithm and the DAVID Bioinformatics Resources database (https://david.ncifcrf.gov/) [17] were used for Gene Ontology (GO) functional analysis of PDE4B genes to understand the biological process of the target, the Kyoto Encyclopedia of Genes and Genomes (KEGG) pathway were used to analyze the main signaling pathways [18].

Immune infiltration analysis

We used the ESTIMATE algorithms to evaluate each TCGA sample by scoring immune cells, tumor purity, and stromal cells [19]. The CIBERSORT algorithm was used to estimate the proportion of different immune cells in cancer tissue, and the differences of immune cells between high and low PDE4B groups in GC tissue were analyzed [20]. We used the "immune gene" module of TIMER 2.0 database [21] (http://timer.cistrome.org/) to explore the relationship between the expression of PDE4B and tumor immune infiltrations.

Statistical analysis

All statistical analyses were conducted on SPSS 19.0 statistical software package, R software (version 4.1.2) and GraphPad Prism 8. The difference between the two groups was analyzed by independent T test. The associations between patient clinical characteristics and PDE4B expression were assessed using the Chi-square test or Trend test. Overall survival was calculated using the Kaplan-Meier method, and survival curves were analyzed using the log-rank test. *P* values < 0.05 were considered statistically significant. The *P* values < 0.05, 0.01, and 0.001 were respectively represented by *, **, and ***.

Results

PDE4B expression in GC tissues

We used the GEPIA2 database to analyze the expression of PDE4B in stomach adenocarcinoma (STAD), which accounts for 95% of GC cases, using normal tissue from the GTEx data set as a control. This analysis included a total of 408 STAD tissues and 211 normal gastric tissues. We found that the gene expression of PDE4B was significantly higher in STAD tissues compared with normal gastric tissues ($P < 0.05$, **Figure 1A**). The expression of PDE4B increased through the pathological stages (stage I/II/III/IV) ($P < 0.05$, **Figure 1B**) and was linked to overall survival rates ($P < 0.05$, **Figure 1C**). To verify this result, we measured the expression of PDE4B mRNA and protein in the human GC cell lines MNK-1, HGC-27 and the human gastric mucosal cell line GES-1. We found that PDE4B mRNA and protein expression in was significantly higher in the GC cell lines ($P < 0.001$, **Figure 1D-F**). To confirm the protein expression of PDE4B in gastric tissue, we conducted immunohistochemical (IHC) analysis on tissue microarrays (TMAs), which comprised 501 GC tissues and 165 adjacent non-tumor tissues. IHC staining revealed that PDE4B was primarily localized to the cytoplasm and demonstrated significant expression in tumor tissue (a staining score ≥ 200 indicates high expression, **Figure 1E**). We found that only 25.45% (42/165) of normal gastric tissues exhibited high expression of PDE4B, whereas in GC tissues, the incidence was 80.84% (405/501) (**Table 1**).

Association between PDE4B expression and clinicopathological characteristics

Our analysis using the GEPIA2 database also revealed a gradual increase in the expression level of PDE4B in STAD tissues across different pathological stages. We investigated the impact of PDE4B on the clinical characteristics of GC patients by examining the association between PDE4B expression and various pathological features (**Table 2**). Our analysis demon-

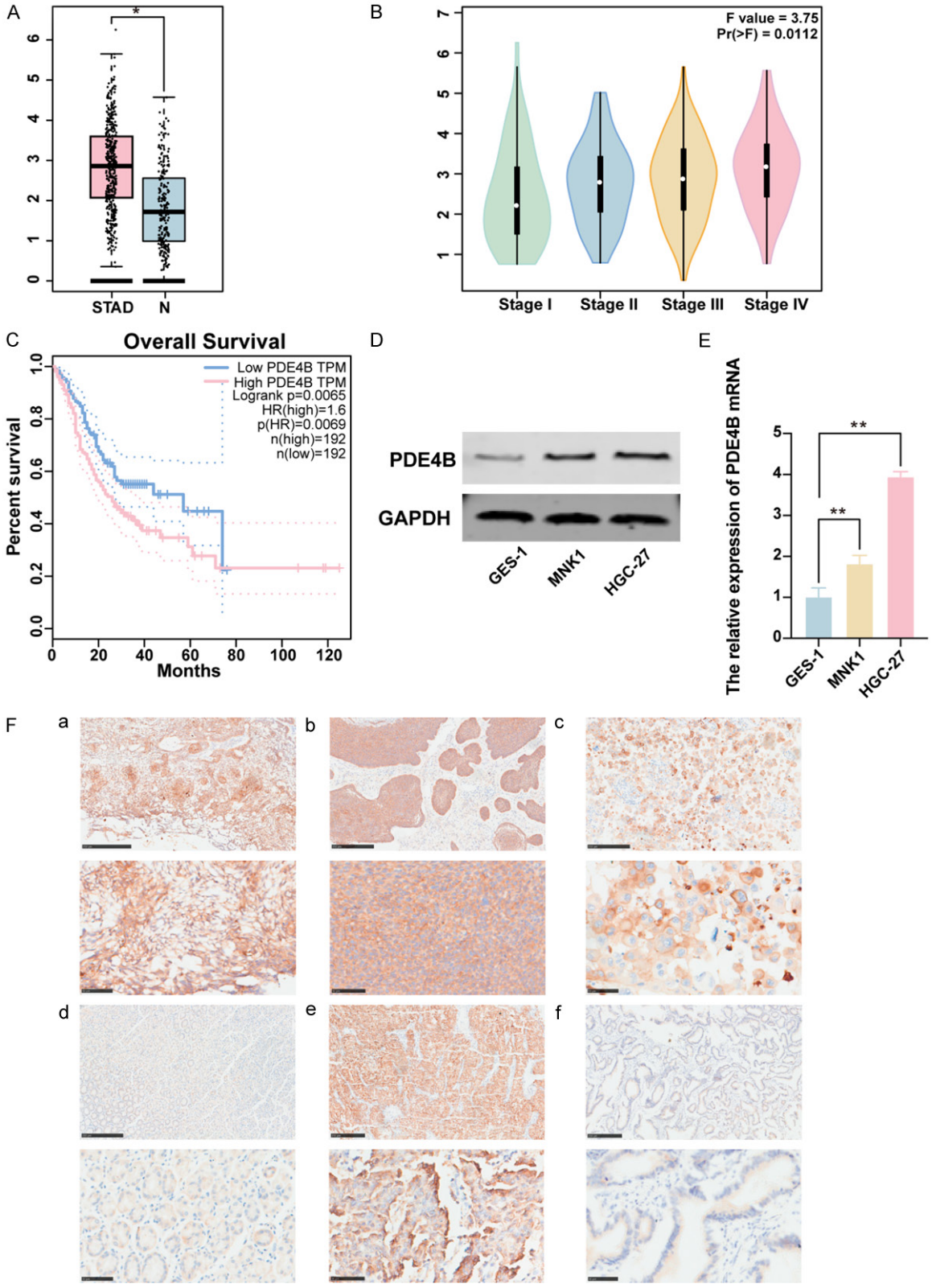

Figure 1. PDE4B expression in GC. A: PDE4B expression in GC tissues and normal tissues in TCGA database. B: PDE4B mRNA expression in GC tissues at different stage. C: Overall survival curves for patients with different PDE4B expression. D, E: Expression of PDE4B in GC and human gastric mucosal cell lines. F: Representative images of PDE4B protein in gastric tissues. a. Low-differentiated squamous carcinoma. b. Well-differentiated squamous carcinoma. c. Signet-ring cell carcinoma. d. Low-differentiated adenocarcinoma. e. Well-differentiated adenocarcinoma. f. Pericarcinomatous tissues. *P < 0.05, **P < 0.01, ***P < 0.001.

Table 1. PDE4B protein expression in gastric mucosa tissues

Characteristics	N	PDE4B expression (%)		χ^2	P
		Low or no	High		
Carcinoma	501	96 (19.16)	405 (80.84)	172.508	< 0.001*
Pericarcinomatous tissue	165	123 (74.55)	42 (25.45)		

*P<0.05.

Table 2. PDE4B protein expression level and GC patient clinicopathological characteristics

Characteristics	N	PDE4B expression		Pearson χ^2	P
		Low or no	High		
Total	501	96 (19.16)	405 (80.84)		
Gender				1.221	0.269
Female	149	33 (22.15)	116 (77.85)		
Male	352	63 (17.90)	289 (82.10)		
Age				0.082	0.774
< 60	168	31 (18.45)	137 (81.55)		
≥ 60	333	65 (19.52)	268 (80.48)		
HP infection				3.520	0.061
Positive	208	48 (23.08)	160 (76.92)		
Negative	293	48 (16.38)	245 (83.62)		
Differentiation				1.182	0.554
Well	142	30 (21.13)	112 (78.87)		
Moderate	207	35 (16.91)	172 (83.09)		
Poor	152	31 (20.39)	121 (79.61)		
Depth of invasion				9.581	0.002*
Tis + T1 + T2	87	27 (31.03)	60 (68.97)		
T3 + T4	414	69 (16.67)	345 (83.33)		
Lymph node metastasis				0.050	0.824
N0	98	48 (18.82)	207 (81.18)		
N1 + N2 + N3	403	48 (19.51)	198 (80.49)		
Distant metastasis				8.474	0.004*
M0	407	88 (21.62)	319 (78.38)		
M1	94	8 (5.51)	86 (91.49)		
TNM stage				29.647	< 0.001*
I	39	20 (51.28)	19 (48.72)		
II	192	29 (15.10)	163 (84.89)		
III	189	36 (19.05)	153 (80.95)		
IV	81	11 (13.58)	70 (86.42)		
Preoperative CEA, ng/ml				0.651	0.420
< 5	201	42 (20.90)	159 (79.10)		
≥ 5	300	54 (18.00)	246 (82.00)		
Preoperative CA199, ng/ml				4.826	0.028*
< 37	201	48 (23.88)	153 (76.12)		
≥ 37	300	48 (16.00)	252 (84.00)		
Her-2				3.721	0.054
Negative	82	22 (26.83)	60 (73.17)		
Positive	419	74 (17.66)	345 (82.34)		

*P < 0.05.

Table 3. Univariate and multivariate analyses of the prognostic factors for overall survival in GC

	Univariate analysis			Multivariate analysis		
	HR	*P*-value	95% CI	HR	*P*-value	95% CI
PDE4B expression						
Low or no vs High	5.254	< 0.001*	3.587-7.696	4.742	< 0.001*	3.226-6.971
Age (year)						
< 60 vs ≥ 60	0.998	0.983	0.804-1.237			
Gender						
Male vs Female	0.966	0.758	0.774-1.206			
Depth of invasion						
Tis + T1 + T2 vs T3 + T4	1.679	0.001*	1.239-2.276			
Lymph node metastasis						
N0 vs N1 + N2 + N3	1.118	0.412	0.857-1.458			
Distant metastasis						
M0 vs M1	3.018	< 0.001*	2.362-3.855	2.049	< 0.001*	1.566-2.682
TNM stage						
I + II vs III + IV	1.295	0.014*	1.054-1.592	1.517	0.001*	1.214-1.894
Differentiation						
Well vs Moderate vs Poor	1.112	0.124	0.971-1.272			
HP infection						
Negative vs Positive	1.729	< 0.001*	1.401-2.133	1.482	0.001*	1.173-1.873
Preoperative CEA, ng/ml						
< 5 vs ≥ 5	1.218	0.064	0.989-1.500			
Preoperative CA199, ng/ml						
< 37 vs ≥ 37	1.748	< 0.001*	1.410-2.165	1.650	< 0.001*	1.330-2.047
Her-2						
Negative vs Positive	1.201	0.203	0.906-1.593			

*$P < 0.05$. HR: Hazard ratio; CI: Confidence interval.

strated significant correlations between PDE4B expression and the following factors: depth of invasion ($\chi^2 = 9.581$, P = 0.002), distant metastasis ($\chi^2 = 8.474$, P = 0.004), TNM stage ($\chi^2 = 29.647$, P < 0.001), and preoperative CA199 levels ($\chi^2 = 4.826$, P = 0.028). Our findings indicate that GC cases with a high expression of PDE4B often progress to more advanced clinical stages with an increased likelihood of distant metastasis when compared with GC cases with low expression of PDE4B.

Relationship between PDE4B expression and prognosis for GC patients

We divided the GEPIA2 database STAD tissue samples into high- and low-expression groups based on the median expression level of PDE4B mRNA. We found that high expression of PDE4B is associated with poor prognosis. By applying univariate analysis to the clinicopathological phenotypes, various risk factors for overall survival (OS) were identified, including PDE4B expression (P < 0.001), depth of invasion (P < 0.001), distant metastasis (P < 0.001), Helicobacter pylori (Hp.) infection (P < 0.001), and preoperative CA199 (P < 0.001) (**Table 3**). These statistically significant factors were then included in a multivariate analysis. The results revealed that high expression of PDE4B (HR: 4.742; 95% CI: 3.226-6.971; P < 0.001), distant metastasis (HR: 2.049; 95% CI: 1.566-2.682; P < 0.001), TNM stage (HR: 1.517; 95% CI: 1.214-1.894; P = 0.001), Hp. infection (HR: 1.482; 95% CI: 1.173-1.873; P = 0.001), and preoperative CA199 (HR: 1.650; 95% CI: 1.330-2.047; P < 0.001) are independent prognostic factors for GC patients (**Figure 2A-E**). These results suggest that PDE4B expression could serve as an independent prognostic biomarker for GC patients and provide valuable insights into predicting GC patient outcomes.

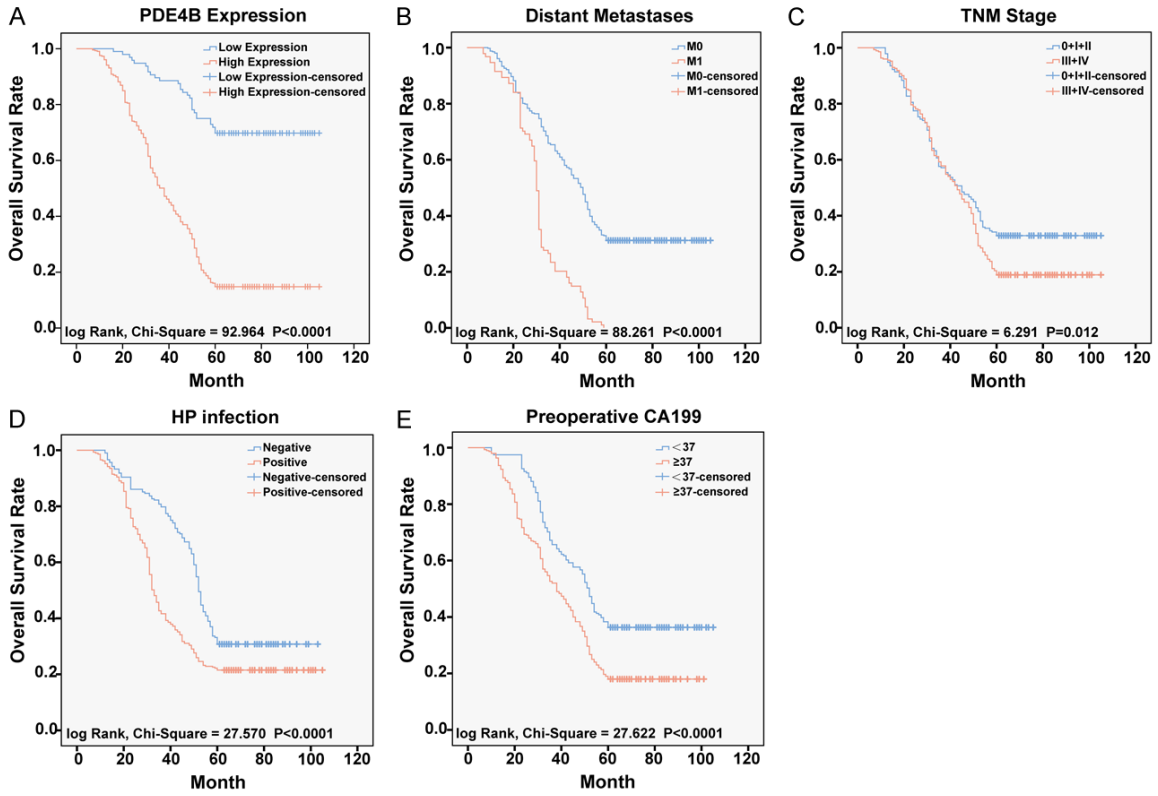

Figure 2. Survival curves of GC patients using the Kaplan-Meier method and the log-rank test. A: Overall survival curves for patients with low PDE4B expression and patients with high PDE4B expression. B: Overall survival curves by distant metastases. C: Overall survival curves by TNM stage. D: Overall survival curves by HP infection. E: Overall survival curves by preoperative CA199.

Decreased PDE4B expression hinders the progression of GC

To investigate the role of PDE4B on GC development, PDE4B expression was knocked down in GC cell lines HGC-27. PDE4B is known to hydrolyze the second messenger cAMP, therefore cAMP level change was examined by WB (**Figure 3A**, **3B**). A cell proliferation (CCK-8) assay showed that down-regulation of PDE4B inhibited the proliferation of GC cells (**Figure 3C**). A subsequent clone formation assay to measure cell survival further confirmed the adverse impact of PDE4B silencing on cell viability (**Figure 3D**). A transwell assay also showed that the knockdown of PDE4B hindered the invasion and migration of GC cells (**Figure 3E**, **3F**).

Flow cytometry demonstrated that apoptosis increased after PDE4B knockdown (**Figure 3G**). Finally, we constructed a tumor xenotransplantation model to determine the role of PDE4B on the development of GC in vivo. The results showed a significant decrease in the volume and weight of subcutaneous tumors in the shPDE4B group (**Figure 3H-J**) compared with controls. These results indicate that the knockdown of PDE4B inhibits the malignant biological characteristics of GC.

Over-expression of PDE4B accelerates the progression of GC

We over-expressed PDE4B in the GC cell line MNK-1 (**Figure 4A**, **4B**). A CCK-8 assay showed that over-expression of PDE4B increased the proliferation of GC cells (**Figure 4C**). A clone formation assay further confirmed the positive effect of PDE4B over-expression on cell viability (**Figure 4D**). Additionally, a transwell migration assay demonstrated that over-expression of PDE4B increased the migratory and invasive abilities of GC cells (**Figure 4E**, **4F**). Flow cytometry showed that apoptosis decreased following PDE4B knockdown (**Figure 4G**). These results strongly suggest that PDE4B overexpression promotes malignancy in GC.

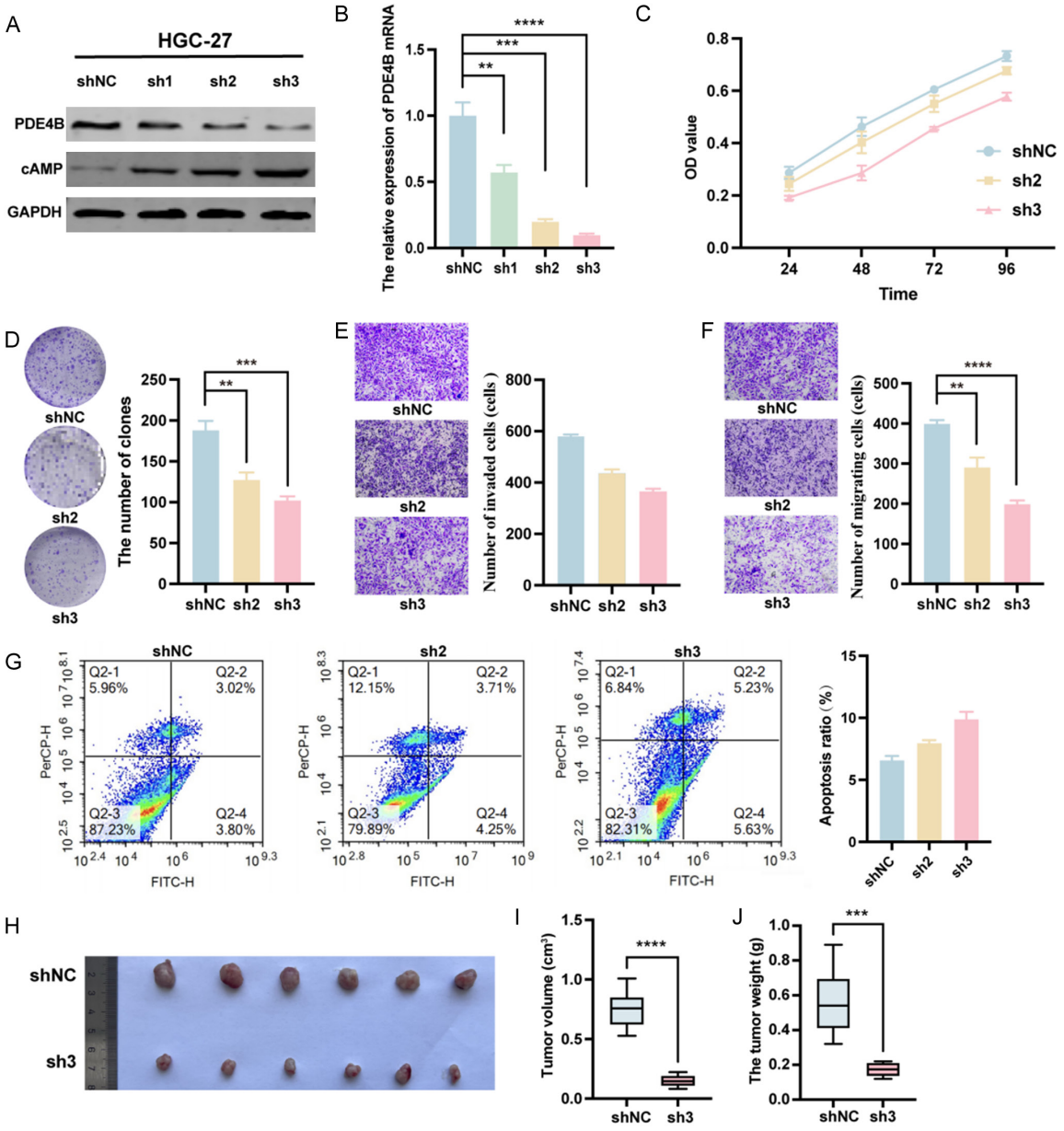

Figure 3. PDE4B plays an oncogenic role in GC cells. A: PDE4B expression of HGC27 cells after shPDE4B transfection. B: PDE4BmRNA expression of HGC-27 cells after shPDE4B transfection. C: The proliferation of GC cells after PDE4B knockdown. D: The clone formation of GC cells after PDE4B silence. E: The invasion of GC cells after downregulation of PDE4B. F: The migration of GC cells after downregulation of PDE4B. G: The apoptosis of GC cells increased after PDE4B knockdown. H: The volumes of tumors in the xenograft mouse model. I, J: The volume and weight of tumors in the xenograft mouse model.

The regulatory mechanism of PDE4B in STAD

To further understand the possible biological function and signal pathway of PDE4B, we used the WGCNA and ESTIMATE algorithms to screen for the co-expression of genes related to PDE4B (**Figure 5A**), selecting the module exhibiting the highest correlation with immune cells and stromal cells. Enrichment analysis was conducted on these 188 genes using the DAVID database. KEGG analysis indicated that the function of PDE4B significantly relates to the cytokine-cytokine receptor interaction, chemokine signaling pathway, B-cell receptor signaling pathway, PI3K-Akt signal pathway and cell adhesion molecules (**Figure 5B**). Gene ontology (GO)

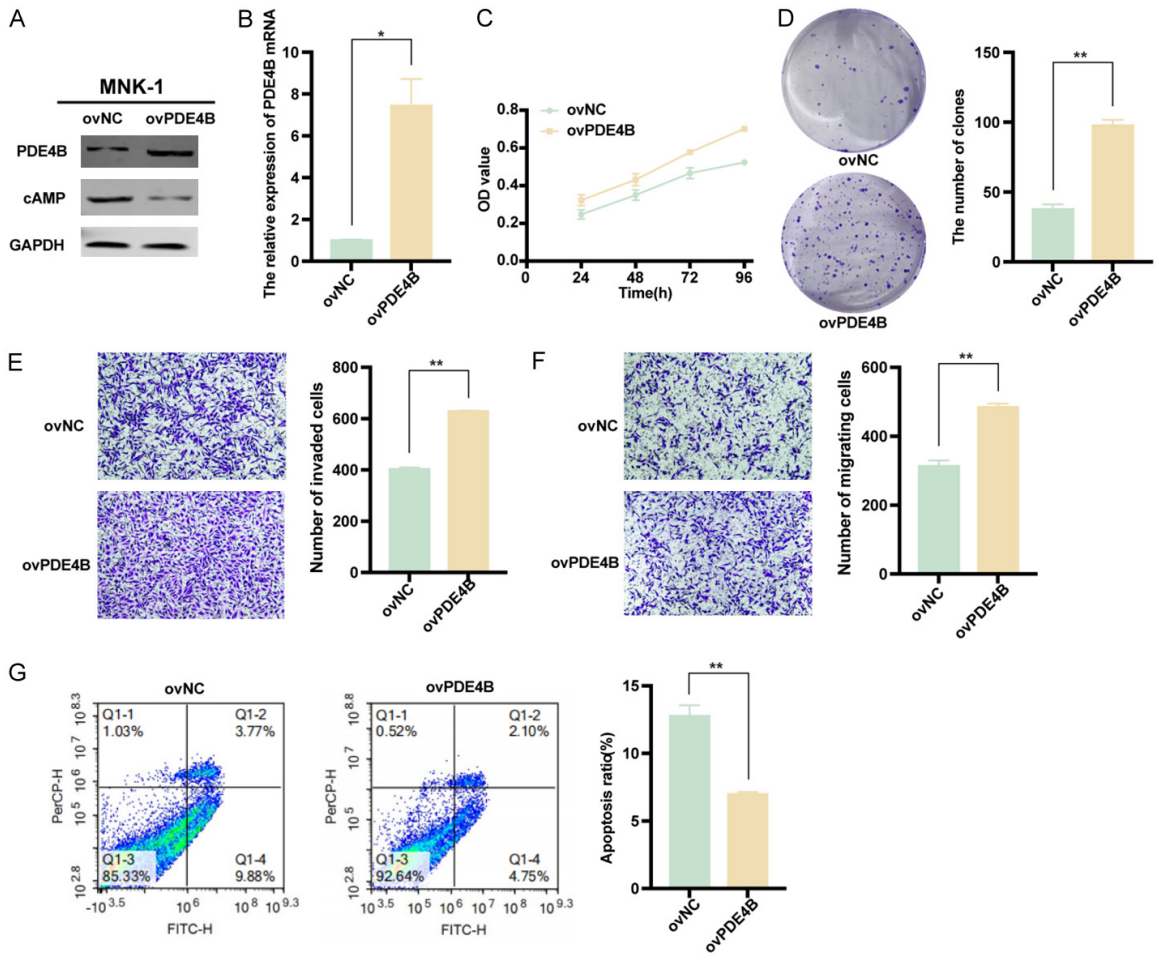

Figure 4. PDE4B plays an oncogenic role in GC cells. A: PDE4B expression of MNK-1 cells after ovPDE4B transfection. B: PDE4BmRNA expression of MNK-1 cells after ovPDE4B transfection. C: The proliferation of GC cells after PDE4B over-expression. D: The clone formation of GC cells after PDE4B over-expression. E: The invasion of GC cells after upregulation of PDE4B. F: The migration of GC cells after upregulation of PDE4B. G: The apoptosis of GC cells decreased after PDE4B over-expression.

analysis showed that the expression of PDE4B may be related to the immune response, signal transduction and cell morphogenesis (**Figure 5C**).

Silencing PDE4B inhibits the PI3K/AKT/MYC pathway

In our preliminary bioinformatic analysis, we observed a potential association between the function of PDE4B and the PI3K/AKT signal pathway. MYC is an important proto-oncogene involved in cell regulation, proliferation, differentiation, and metabolism, and is also a downstream actor in the PI3K/AKT pathway. To further investigate the role of PDE4B in GC, western blot analysis confirmed that silencing PDE4B reduced MYC expression. Furthermore, upon down-regulation of PDE4B expression, we found that phosphorylation of the PI3K/AKT pathway was inhibited. Conversely, over-expression of PDE4B led to increased levels of MYC and enhanced phosphorylation of the PI3K/AKT pathway (**Figure 5D**). Using a PI3K inhibitor, wortmannin, reversed the effect of over-expression of PDE4B on cell proliferation, migration, and invasion (**Figure 5E**, **5F**). In summary, these findings suggest that PDE4B promotes GC progression through activation of the PI3K/AKT/MYC pathway.

PDE4B expression is related to immune cell infiltration

Studies have shown that the infiltration of immune cells into the tumor microenvironment

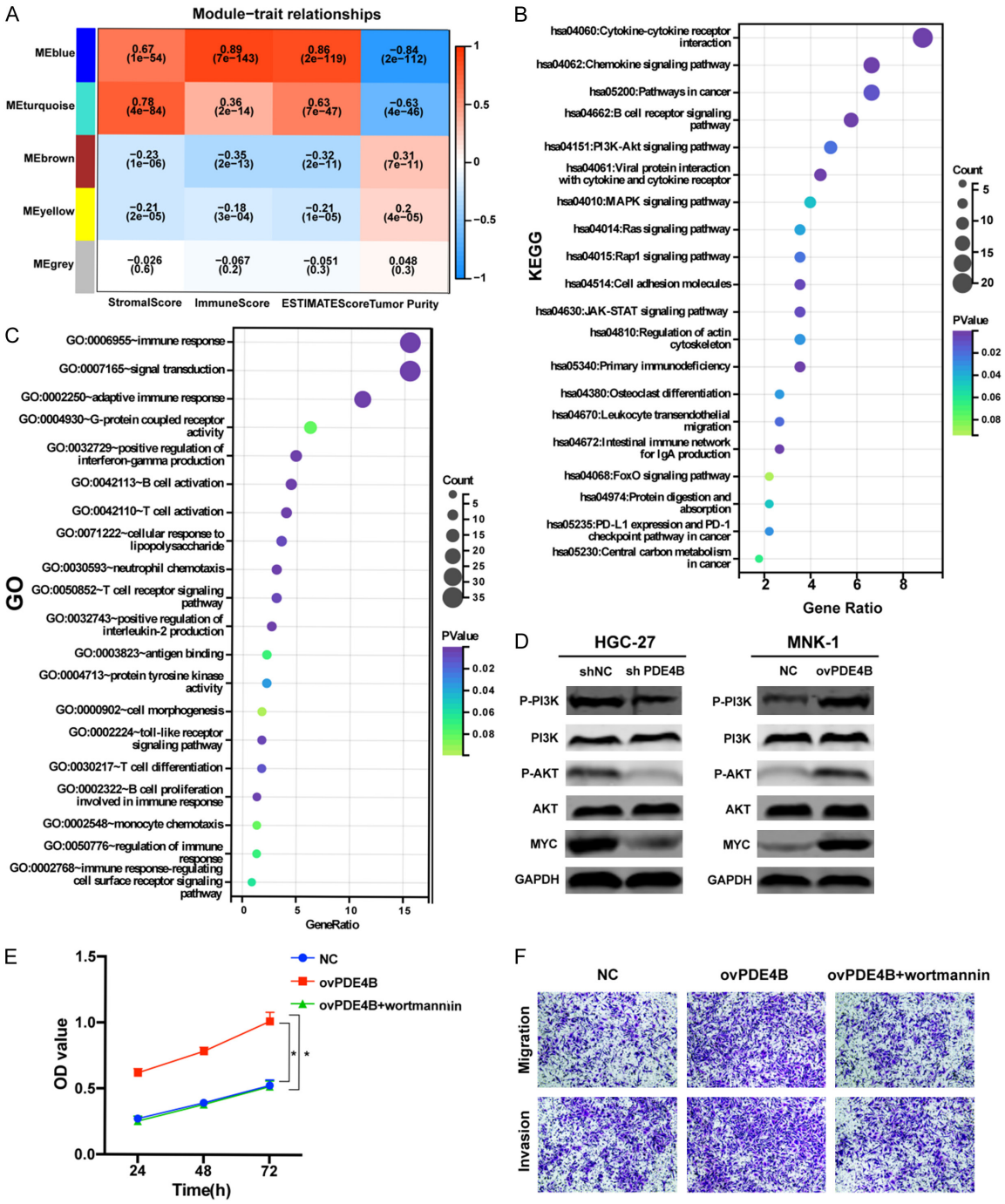

Figure 5. Expression and phosphorylation of PI3K/AKT/MYC. A: WGCNA heatmap. B, C: KEGG and GO were used for enrichment analysis of PDE4B. D: Expression and phosphorylation of PI3K/AKT/MYC pathways in shPDE4B and ovPDE4B cells compared with the control. E: The proliferation of GC cells after wortmannin treatment. F: The migration and invasion of GC cells after wortmannin treatment.

(TME) plays an important role in regulating tumor occurrence, development, and prognosis [22]. Our GO analysis also found that PDE4B is associated with immunity. Therefore, we used the ESTIMATE algorithm to measure the correlation between PDE4B and immune cell infiltration. The results showed that PDE4B was positively correlated with immune score ($P < 0.0001$, $r = 0.63$) and stromal score ($P < 0.0001$, $r = 0.64$) (**Figure 6A**, **6B**). These results

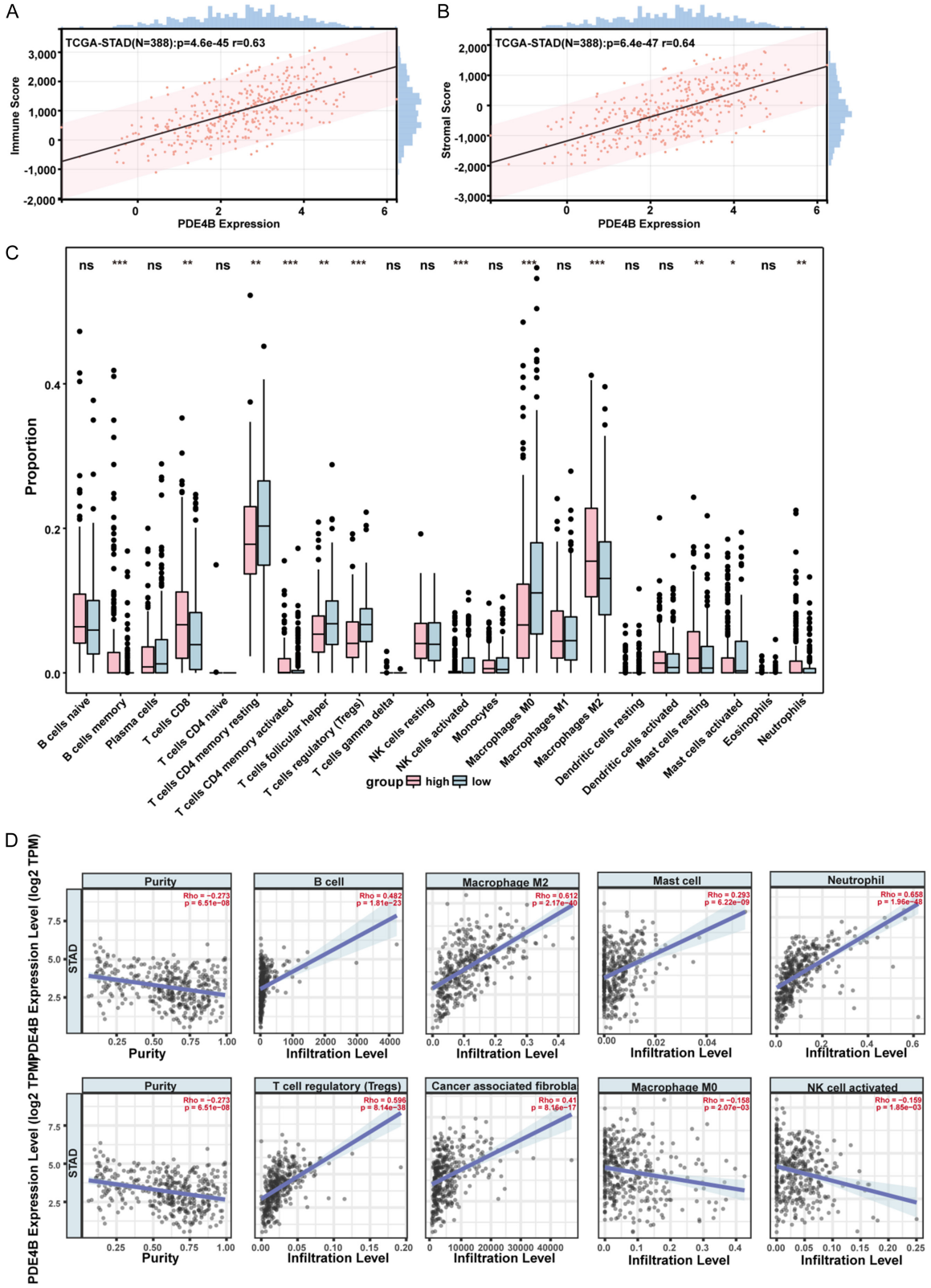

Figure 6. The correlation between PDE4B and immune cell infiltration. A: The expression of PDE4B was significantly correlated with immune scores. B: The expression of PDE4B was significantly correlated with stromal scores. C: The correlation between PDE4BmRNA and immune cells (CIBERSORT). D: The correlation between PDE4BmRNA and immune cell infiltration in the TIMER2.0 database.

Table 4. PDE4B protein expression level and immune cell infiltration in TME

Characteristics	N	PDE4B expression		Pearson χ^2	P
		Low or no	High		
Total	276	51 (18.48)	225 (81.52)		
CD19				5.666	0.017*
Low or no	86	23 (26.74)	63 (73.26)		
High	190	28 (14.74)	162 (85.26)		
CD117				2.807	0.097
Low or no	112	26 (23.21)	86 (76.79)		
High	164	25 (15.24)	139 (84.76)		
SMA				13.140	< 0.001*
Low or no	53	19 (23.08)	34 (76.92)		
High	233	32 (16.38)	191 (83.62)		

*P<0.05.

suggest that the expression level of PDE4B may be related to the infiltration of immune cells into the TME of GC.

Subsequently, we used CIBERSORT to calculate the proportion and expression of different immune cell types in TCGA-STAD tissue (**Figure 6C**). The results showed that the high expression of PDE4B was related to the infiltration of various types of immune cells, including memory B cells, CD8+ T cells, CD4+ T cells, T follicular helper cells, T regulatory cells (Tregs), activated natural killer (NK) cells, M0 macrophages, M2 macrophages, mast cells, and neutrophils ($P < 0.05$).

We further investigated the correlation between PDE4B mRNA expression and specific immune cell infiltration ugh the TIMER2.0 database (**Figure 6D**). We found that PDE4B was significantly positively correlated with the infiltration of B cells (R = 0.482, P = 1.81e-23), M2 Macrophages (R = 0.612, P = 2.17e-40), Mast cells (R = 0.293, P = 6.22e-09), neutrophils (R = 0.658, P = 1.96e-48), Tregs (R = -0.196, P = 1.20e-04) and cancer-associated fibroblasts (R = 0.41, P = 8.16e-17), while it was significantly negatively correlated with the infiltration of M0 macrophages (R = -0.158, P = 2.07e-03), activated NK cells (R = -0.159, P = 1.85e-03).

We selected three immune cell types for validation via IHC staining: B cells, mast cells, and cancer-associated fibroblasts. We then conducted correlation analysis with the expression of PDE4B. We found that the expression of CD19, a B-cell marker, was positively correlated with the expression of PDE4B ($\chi^2 = 5.666$, P = 0.017). The expression of CD117, a mast cell marker, was positively correlated with the expression of PDE4B. And the expression of SMA, a cancer-associated fibroblast marker, was significantly positively correlated with the expression of PDE4B ($\chi^2 = 13.140$, $P < 0.001$) (a staining score ≥ 200 indicates high expression, **Table 4**).

Discussion

Phosphodiesterase-4 (PDE4) has four isoforms, and PDE4B plays a crucial role in the diagnosis, classification, treatment, and prognosis of various cancers [23]. The expression level of PDE4B mRNA is significantly elevated in hematologic malignancies [12, 24-26], glioblastoma [27, 28], neuroblastoma [29], melanoma [30], esophageal cancer [31], colorectal cancer [32], and lung cancer [33]. Furthermore, PDE4B expression is associated with colorectal cancer recurrence [15], and anti-apoptotic activity and metastasis in endometrial cancer [14] and renal cell carcinoma [13]. It has also been associated with tumor heterogeneity changes in inflammatory breast cancer [34]. PDE4B can promote cell migration and invasion during bladder cancer by inducing epithelial-mesenchymal transition [35]. Increased expression of PDE4B has been observed in lung adenocarcinoma and is correlated with the prognosis and immune infiltration of LUAD [36]. Numerous studies and clinical data have demonstrated that PDE4B inhibitors can enhance cancer cell apoptosis and inhibit cancer cell proliferation, transformation, and migration. In this study, we analyzed bioinformatic data, clinical pathological information, and experimental validation,

and found that PDE4B mRNA is highly expressed in GC cells. The protein expression rate of PDE4B in GC tissues is higher than in normal gastric tissues. This high level of PDE4B expression is significantly associated with deep invasion, distant metastasis, TNM stage, and preoperative CA199 levels. GC patients with high expression of PDE4B tend to be in a more advanced clinical stage, exhibit distant metastasis, and have significantly decreased OS. We have experimentally confirmed that down-regulation of PDE4B significantly inhibits the proliferation, migration, and invasion of GC cells in vitro and in vivo. Conversely, over-expression of PDE4B accelerates the malignant biological functions of GC, promoting GC development. These findings suggest that PDE4B promotes the progression of GC and is significantly positively associated with poor prognosis in GC patients. It may serve as a new prognostic biomarker and therapeutic target for GC.

Extensive research has confirmed that PDE4B is a critical regulator of intracellular cAMP levels [37, 38]. The cAMP/PDE4 pathway participates in inflammation and immune regulation and is involved in the development of various cancer-related pathways. PDE4 serves as an anti-angiogenic target in diffuse large B-cell lymphoma (DLBCL), and PDE4B affects the cAMP-mediated inhibition of the PI3K/AKT signaling pathway, leading to the down-regulation of vascular endothelial growth factor secretion. This pathway may play an important role in the pathogenesis of hematologic malignancies [24]. Additionally, KEGG and GO enrichment analysis showed that the regulatory mechanisms of PDE4B may be linked with the PI3K/AKT pathway. Extensive evidence suggests that the PI3K/Akt pathway plays a vital role in various cellular processes, including tumor proliferation, apoptosis, angiogenesis, and metastasis [39]. The MYC protein acts as a downstream protein of the PI3K/AKT pathway [40], and functions as a transcription factor involved in cell proliferation, apoptosis, differentiation, and metabolism [41]. MYC is a major oncogene in humans [42]. The correlation between PDE4B and MYC in GC tissues was confirmed by western blot analysis, which demonstrated that silencing PDE4B led to the suppression of MYC expression. Upon knockdown and over-expression of PDE4B, the expression and phosphorylation levels of the PI3K/AKT pathway were analyzed. It was found that PDE4B significantly enhanced the phosphorylation levels of the PI3K/AKT pathway. These findings suggest that PDE4B regulates MYC expression through the PI3K/AKT pathway, thereby influencing the progression of GC.

Given the important role of immune cells in tumorigenesis, development, and metastasis within the TME, this study employed the CIBERSORT algorithm and TIMER 2.0 database to interrogate the role of PDE4B in immune cell activity during GC. It was found that a high expression level of PDE4B mRNA was significantly positively correlated with M2 macrophages, regulatory T cells (Treg), cancer-associated fibroblasts, B cells, mast cells, and neutrophils. Conversely, it was significantly negatively correlated with M0 macrophages and activated NK cell infiltration.

There are various subtypes of immune cells present in the TME, and research has indicated that certain subtypes of immune cells are associated with tumor progression and adverse prognosis. Examples of these subtypes include M2 macrophages, Treg cells, and cancer-associated fibroblasts [43-45]. Furthermore, studies have suggested that B-cell infiltration may be associated with tumor metastasis and can enhance tumor activity through the production of immunosuppressive cytokines [46, 47]. Additionally, mast cells play a role in promoting tumor development by releasing angiogenic and lymphangiogenic factors [48] that reshape the TME [49]. Neutrophils can release reactive oxygen species (ROS) [50, 51] and contribute to immune evasion [52], thereby facilitating tumor proliferation [53, 54], tumor cell migration, and suppressing anti-tumor T-cell responses [55]. Research has shown that high relative infiltration abundance of M0 macrophages is associated with improved tumor prognosis and treatment efficacy [56]. NK cells are involved in antiviral and anti-tumor immunity and have emerged as promising therapeutic targets for several solid tumors and hematologic malignancies [57]. Based on these findings, we speculate that the high expression of PDE4B in GC tissues may promote tumor occurrence and development by reshaping the TME and impacting the effectiveness of immunotherapy.

This study demonstrates that PDE4B is highly expressed in GC cells and is significantly posi-

tively correlated with poor prognosis in GC. PDE4B promotes proliferation, colony formation, migration, and invasion by GC cells by regulating the PI3K/AKT/MYC pathway and immune cell infiltration into the TME. Therefore, PDE4B may serve as a new prognostic biomarker and therapeutic target for GC patients.

Acknowledgements

This work was supported by grants from the Natural Science Foundation of Inner Mongolia Autonomous Region (2021LHMS08046). We thank Bevin McGeever, PhD, from Liwen Bianji (Edanz) (www.liwenbianji.cn), for editing the English text of a draft of this manuscript.

All the participants signed an informed consent form.

Disclosure of conflict of interest

None.

Address correspondence to: Dr. Qun Hu, Department of Oncology, Affiliated Hospital of Inner Mongolia Medical University, No. 1 Tongdao North Road, Hohhot 010050, Inner Mongolia, China. E-mail: huqun2015@126.com

References

[1] Xie J, Pang Y and Wu X. Taxifolin suppresses the malignant progression of gastric cancer by regulating the AhR/CYP1A1 signaling pathway. Int J Mol Med 2021; 48: 197.

[2] Chen W, Zheng R, Baade PD, Zhang S, Zeng H, Bray F, Jemal A, Yu XQ and He J. Cancer statistics in China, 2015. CA Cancer J Clin 2016; 66: 115-132.

[3] Smyth EC, Nilsson M, Grabsch HI, van Grieken NC and Lordick F. Gastric cancer. Lancet 2020; 396: 635-648.

[4] Saito H, Fukumoto Y, Osaki T, Fukuda K, Tatebe S, Tsujitani S and Ikeguchi M. Distinct recurrence pattern and outcome of adenocarcinoma of the gastric cardia in comparison with carcinoma of other regions of the stomach. World J Surg 2006; 30: 1864-1869.

[5] Wagner AD, Syn NL, Moehler M, Grothe W, Yong WP, Tai BC, Ho J and Unverzagt S. Chemotherapy for advanced gastric cancer. Cochrane Database Syst Rev 2017; 8: CD004064.

[6] Houslay MD and Adams DR. PDE4 cAMP phosphodiesterases: modular enzymes that orchestrate signalling cross-talk, desensitization and compartmentalization. Biochem J 2003; 370: 1-18.

[7] Lebwohl MG, Kircik LH, Moore AY, Stein Gold L, Draelos ZD, Gooderham MJ, Papp KA, Bagel J, Bhatia N, Del Rosso JQ, Ferris LK, Green LJ, Hebert AA, Jones T, Kempers SE, Pariser DM, Yamauchi PS, Zirwas M, Albrecht L, Devani AR, Lomaga M, Feng A, Snyder S, Burnett P, Higham RC and Berk DR. Effect of roflumilast cream vs vehicle cream on chronic plaque psoriasis: the DERMIS-1 and DERMIS-2 randomized clinical trials. JAMA 2022; 328: 1073-1084.

[8] Maier C, Ramming A, Bergmann C, Weinkam R, Kittan N, Schett G, Distler JHW and Beyer C. Inhibition of phosphodiesterase 4 (PDE4) reduces dermal fibrosis by interfering with the release of interleukin-6 from M2 macrophages. Ann Rheum Dis 2017; 76: 1133-1141.

[9] Lipworth BJ. Phosphodiesterase-4 inhibitors for asthma and chronic obstructive pulmonary disease. Lancet 2005; 365: 167-175.

[10] Richeldi L, Azuma A, Cottin V, Hesslinger C, Stowasser S, Valenzuela C, Wijsenbeek MS, Zoz DF, Voss F and Maher TM; 1305-0013 Trial Investigators. Trial of a preferential phosphodiesterase 4B inhibitor for idiopathic pulmonary fibrosis. N Engl J Med 2022; 386: 2178-2187.

[11] Kim SW, Rai D, McKeller MR and Aguiar RC. Rational combined targeting of phosphodiesterase 4B and SYK in DLBCL. Blood 2009; 113: 6153-6160.

[12] Smith PG, Wang F, Wilkinson KN, Savage KJ, Klein U, Neuberg DS, Bollag G, Shipp MA and Aguiar RC. The phosphodiesterase PDE4B limits cAMP-associated PI3K/AKT-dependent apoptosis in diffuse large B-cell lymphoma. Blood 2005; 105: 308-316.

[13] Holloway DT, Kon M and DeLisi C. In silico regulatory analysis for exploring human disease progression. Biol Direct 2008; 3: 24.

[14] Dong P, Xiong Y, Yue J, Xu D, Ihira K, Konno Y, Kobayashi N, Todo Y and Watari H. Long noncoding RNA NEAT1 drives aggressive endometrial cancer progression via miR-361-regulated networks involving STAT3 and tumor microenvironment-related genes. J Exp Clin Cancer Res 2019; 38: 295.

[15] Tsunoda T, Ota T, Fujimoto T, Doi K, Tanaka Y, Yoshida Y, Ogawa M, Matsuzaki H, Hamabashiri M, Tyson DR, Kuroki M, Miyamoto S and Shirasawa S. Inhibition of phosphodiesterase-4 (PDE4) activity triggers luminal apoptosis and AKT dephosphorylation in a 3-D colonic-crypt model. Mol Cancer 2012; 11: 46.

[16] Tang Z, Kang B, Li C, Chen T and Zhang Z. GEPIA2: an enhanced web server for large-scale expression profiling and interactive analysis. Nucleic Acids Res 2019; 47: W556-W560.

[17] Sherman BT, Hao M, Qiu J, Jiao X, Baseler MW, Lane HC, Imamichi T and Chang W. DAVID: a

web server for functional enrichment analysis and functional annotation of gene lists (2021 update). Nucleic Acids Res 2022; 50: W216-W221.

[18] Subramanian A, Tamayo P, Mootha VK, Mukherjee S, Ebert BL, Gillette MA, Paulovich A, Pomeroy SL, Golub TR, Lander ES and Mesirov JP. Gene set enrichment analysis: a knowledge-based approach for interpreting genome-wide expression profiles. Proc Natl Acad Sci U S A 2005; 102: 15545-15550.

[19] Zhang C, Zheng JH, Lin ZH, Lv HY, Ye ZM, Chen YP and Zhang XY. Profiles of immune cell infiltration and immune-related genes in the tumor microenvironment of osteosarcoma. Aging (Albany NY) 2020; 12: 3486-3501.

[20] Jiang S, Zhang Y, Zhang X, Lu B, Sun P, Wu Q, Ding X and Huang J. GARP correlates with tumor-infiltrating T-cells and predicts the outcome of gastric cancer. Front Immunol 2021; 12: 660397.

[21] Li T, Fu J, Zeng Z, Cohen D, Li J, Chen Q, Li B and Liu XS. TIMER2.0 for analysis of tumor-infiltrating immune cells. Nucleic Acids Res 2020; 48: W509-W514.

[22] Ren N, Liang B and Li Y. Identification of prognosis-related genes in the tumor microenvironment of stomach adenocarcinoma by TCGA and GEO datasets. Biosci Rep 2020; 40: BSR20200980.

[23] Miao Y, Peng L, Chen Z, Hu Y, Tao L, Yao Y, Wu Y, Yang D and Xu T. Recent advances of phosphodiesterase 4B in cancer. Expert Opin Ther Targets 2023; 27: 121-132.

[24] Suhasini AN, Wang L, Holder KN, Lin AP, Bhatnagar H, Kim SW, Moritz AW and Aguiar RCT. A phosphodiesterase 4B-dependent interplay between tumor cells and the microenvironment regulates angiogenesis in B-cell lymphoma. Leukemia 2016; 30: 617-626.

[25] Kim SW, Rai D and Aguiar RC. Gene set enrichment analysis unveils the mechanism for the phosphodiesterase 4B control of glucocorticoid response in B-cell lymphoma. Clin Cancer Res 2011; 17: 6723-6732.

[26] Yang JJ, Cheng C, Devidas M, Cao X, Campana D, Yang W, Fan Y, Neale G, Cox N, Scheet P, Borowitz MJ, Winick NJ, Martin PL, Bowman WP, Camitta B, Reaman GH, Carroll WL, Willman CL, Hunger SP, Evans WE, Pui CH, Loh M and Relling MV. Genome-wide association study identifies germline polymorphisms associated with relapse of childhood acute lymphoblastic leukemia. Blood 2012; 120: 4197-4204.

[27] Moon EY, Lee GH, Lee MS, Kim HM and Lee JW. Phosphodiesterase inhibitors control A172 human glioblastoma cell death through cAMP-mediated activation of protein kinase A and Epac1/Rap1 pathways. Life Sci 2012; 90: 373-380.

[28] Dixit D, Prager BC, Gimple RC, Miller TE, Wu Q, Yomtoubian S, Kidwell RL, Lv D, Zhao L, Qiu Z, Zhang G, Lee D, Park DE, Wechsler-Reya RJ, Wang X, Bao S and Rich JN. Glioblastoma stem cells reprogram chromatin in vivo to generate selective therapeutic dependencies on DPY30 and phosphodiesterases. Sci Transl Med 2022; 14: eabf3917.

[29] Jang IS and Juhnn YS. Adaptation of cAMP signaling system in SH-SY5Y neuroblastoma cells following expression of a constitutively active stimulatory G protein alpha, Q227L Gsalpha. Exp Mol Med 2001; 33: 37-45.

[30] Marquette A, André J, Bagot M, Bensussan A and Dumaz N. ERK and PDE4 cooperate to induce RAF isoform switching in melanoma. Nat Struct Mol Biol 2011; 18: 584-591.

[31] Ye B, Fan D, Xiong W, Li M, Yuan J, Jiang Q, Zhao Y, Lin J, Liu J, Lv Y, Wang X, Li Z, Su J and Qiao Y. Oncogenic enhancers drive esophageal squamous cell carcinogenesis and metastasis. Nat Commun 2021; 12: 4457.

[32] Kim DU, Kwak B and Kim SW. Phosphodiesterase 4B is an effective therapeutic target in colorectal cancer. Biochem Biophys Res Commun 2019; 508: 825-831.

[33] He RQ, Li XJ, Liang L, Xie Y, Luo DZ, Ma J, Peng ZG, Hu XH and Chen G. The suppressive role of miR-542-5p in NSCLC: the evidence from clinical data and in vivo validation using a chick chorioallantoic membrane model. BMC Cancer 2017; 17: 655.

[34] Luo R, Chong W, Wei Q, Zhang Z, Wang C, Ye Z, Abu-Khalaf MM, Silver DP, Stapp RT, Jiang W, Myers RE, Li B, Cristofanilli M and Yang H. Whole-exome sequencing identifies somatic mutations and intratumor heterogeneity in inflammatory breast cancer. NPJ Breast Cancer 2021; 7: 72.

[35] Huang Z, Liu J, Yang J, Yan Y, Yang C, He X, Huang R, Tan M, Wu D, Yan J and Shen B. PDE4B induces epithelial-to-mesenchymal transition in bladder cancer cells and is transcriptionally suppressed by CBX7. Front Cell Dev Biol 2021; 9: 783050.

[36] Tong L, Shan M, Zou W, Liu X, Felsher DW and Wang J. Cyclic adenosine monophosphate/phosphodiesterase 4 pathway associated with immune infiltration and PD-L1 expression in lung adenocarcinoma cells. Front Oncol 2022; 12: 904969.

[37] Millar JK, Pickard BS, Mackie S, James R, Christie S, Buchanan SR, Malloy MP, Chubb JE, Huston E, Baillie GS, Thomson PA, Hill EV, Brandon NJ, Rain JC, Camargo LM, Whiting PJ, Houslay MD, Blackwood DH, Muir WJ and Porteous DJ. DISC1 and PDE4B are interacting

genetic factors in schizophrenia that regulate cAMP signaling. Science 2005; 310: 1187-1191.
[38] Huang B, Chen Z, Geng L, Wang J, Liang H, Cao Y, Chen H, Huang W, Su M, Wang H, Xu Y, Liu Y, Lu B, Xian H, Li H, Li H, Ren L, Xie J, Ye L, Wang H, Zhao J, Chen P, Zhang L, Zhao S, Zhang T, Xu B, Che D, Si W, Gu X, Zeng L, Wang Y, Li D, Zhan Y, Delfouneso D, Lew AM, Cui J, Tang WH, Zhang Y, Gong S, Bai F, Yang M and Zhang Y. Mucosal profiling of pediatric-onset colitis and IBD reveals common pathogenics and therapeutic pathways. Cell 2019; 179: 1160-1176, e1124.
[39] He Y, Sun MM, Zhang GG, Yang J, Chen KS, Xu WW and Li B. Targeting PI3K/Akt signal transduction for cancer therapy. Signal Transduct Target Ther 2021; 6: 425.
[40] Zhang F, Li K, Yao X, Wang H, Li W, Wu J, Li M, Zhou R, Xu L and Zhao L. A miR-567-PIK3AP1-PI3K/AKT-c-Myc feedback loop regulates tumour growth and chemoresistance in gastric cancer. EBioMedicine 2019; 44: 311-321.
[41] Chen H, Liu H and Qing G. Targeting oncogenic Myc as a strategy for cancer treatment. Signal Transduct Target Ther 2018; 3: 5.
[42] Baluapuri A, Wolf E and Eilers M. Target gene-independent functions of MYC oncoproteins. Nat Rev Mol Cell Biol 2020; 21: 255-267.
[43] Chen Z, Zhou L, Liu L, Hou Y, Xiong M, Yang Y, Hu J and Chen K. Single-cell RNA sequencing highlights the role of inflammatory cancer-associated fibroblasts in bladder urothelial carcinoma. Nat Commun 2020; 11: 5077.
[44] Marshall EA, Ng KW, Kung SH, Conway EM, Martinez VD, Halvorsen EC, Rowbotham DA, Vucic EA, Plumb AW, Becker-Santos DD, Enfield KS, Kennett JY, Bennewith KL, Lockwood WW, Lam S, English JC, Abraham N and Lam WL. Emerging roles of T helper 17 and regulatory T cells in lung cancer progression and metastasis. Mol Cancer 2016; 15: 67.
[45] Xia Y, Rao L, Yao H, Wang Z, Ning P and Chen X. Engineering macrophages for cancer immunotherapy and drug delivery. Adv Mater 2020; 32: e2002054.
[46] Gu Y, Liu Y, Fu L, Zhai L, Zhu J, Han Y, Jiang Y, Zhang Y, Zhang P, Jiang Z, Zhang X and Cao X. Tumor-educated B cells selectively promote breast cancer lymph node metastasis by HSPA4-targeting IgG. Nat Med 2019; 25: 312-322.
[47] Horikawa M, Minard-Colin V, Matsushita T and Tedder TF. Regulatory B cell production of IL-10 inhibits lymphoma depletion during CD20 immunotherapy in mice. J Clin Invest 2011; 121: 4268-4280.
[48] Sammarco G, Varricchi G, Ferraro V, Ammendola M, De Fazio M, Altomare DF, Luposella M, Maltese L, Currò G, Marone G, Ranieri G and Memeo R. Mast cells, angiogenesis and lymphangiogenesis in human gastric cancer. Int J Mol Sci 2019; 20: 2106.
[49] Huang B, Lei Z, Zhang GM, Li D, Song C, Li B, Liu Y, Yuan Y, Unkeless J, Xiong H and Feng ZH. SCF-mediated mast cell infiltration and activation exacerbate the inflammation and immunosuppression in tumor microenvironment. Blood 2008; 112: 1269-1279.
[50] Knaapen AM, Seiler F, Schilderman PA, Nehls P, Bruch J, Schins RP and Borm PJ. Neutrophils cause oxidative DNA damage in alveolar epithelial cells. Free Radic Biol Med 1999; 27: 234-240.
[51] Wculek SK, Bridgeman VL, Peakman F and Malanchi I. Early neutrophil responses to chemical carcinogenesis shape long-term lung cancer susceptibility. iScience 2020; 23: 101277.
[52] Kargl J, Busch SE, Yang GH, Kim KH, Hanke ML, Metz HE, Hubbard JJ, Lee SM, Madtes DK, McIntosh MW and Houghton AM. Neutrophils dominate the immune cell composition in non-small cell lung cancer. Nat Commun 2017; 8: 14381.
[53] Cristinziano L, Modestino L, Loffredo S, Varricchi G, Braile M, Ferrara AL, de Paulis A, Antonelli A, Marone G and Galdiero MR. Anaplastic thyroid cancer cells induce the release of mitochondrial extracellular DNA traps by viable neutrophils. J Immunol 2020; 204: 1362-1372.
[54] Antonio N, Bønnelykke-Behrndtz ML, Ward LC, Collin J, Christensen IJ, Steiniche T, Schmidt H, Feng Y and Martin P. The wound inflammatory response exacerbates growth of pre-neoplastic cells and progression to cancer. EMBO J 2015; 34: 2219-2236.
[55] Coffelt SB, Kersten K, Doornebal CW, Weiden J, Vrijland K, Hau CS, Verstegen NJM, Ciampricotti M, Hawinkels LJAC, Jonkers J and de Visser KE. IL-17-producing γδ T cells and neutrophils conspire to promote breast cancer metastasis. Nature 2015; 522: 345-348.
[56] Yan C, Li K, Meng F, Chen L, Zhao J, Zhang Z, Xu D, Sun J and Zhou M. Integrated immunogenomic analysis of single-cell and bulk tissue transcriptome profiling unravels a macrophage activation paradigm associated with immunologically and clinically distinct behaviors in ovarian cancer. J Adv Res 2023; 44: 149-160.
[57] Crinier A, Narni-Mancinelli E, Ugolini S and Vivier E. SnapShot: natural killer cells. Cell 2020; 180: 1280-1280, e1281.